Terr. Atmos. Ocean. Sci., Vol. 23, No. 1, 25-38, February 2012 doi: 10.3319/TAO.2011.06.30.02(A)

The Influence of Meteorological Conditions and Complex Topography on Ozone Concentrations in a Valley Area near Coastal Metropolitan Cities

Jae-Eun Kang, Sang-Keun Song, Hwa Woon Lee, and Yoo-Keun Kim *

Division of Earth Environmental System, Pusan National University, Busan, Republic of Korea

Received 25 January 2011, accepted 30 June 2011

ABSTRACT

The influences of meteorological conditions and complex topography on ozone (O_3) concentrations were evaluated at two different sites [Jung Ang (JA): a semi-closed topography and Seo Chang (SC): a closed topography] within a valley city neighboring coastal metropolitan cities (Busan and Ulsan) during days exhibiting high O_3 episodes (8 and 10 August 2006), using the MM5-CMAQ modeling system. The contributions of physical and chemical processes to the O_3 concentrations were also assessed within the mixed layers of the two sites (JA and SC) during the study period. High O_3 concentrations at site JA on 8 August were the result of combined effects of the horizontal transport (in a north-south direction) of O_3 and its precursors and their subsequent reaction with southerly (from Busan) and easterly sea breezes (from Ulsan) and their accumulation due to the convergence of these sea breezes. Such O_3 enhancements on 10 August were caused mainly by the vertical transport of O_3 and its precursors and partly by their accumulation (from local emission sources) due to weak winds. Unlike site JA, the O_3 enhancement at site SC on 8 August was mainly ascribable to horizontal transport (in an east-west direction) from the source regions of Ulsan. On 10 August, vertical transport of downslope flows from the top of mountains largely contributed to O_3 concentrations. In addition, the heights of maximum O_3 inflow due to horizontal or vertical transport between the two sites during the episodes were different depending on the differences in the heights of mountains and/or the movement directions and intensities of sea breezes.

Key words: Valley city, Meteorological conditions, Topographical features, O_3, Process analysis

Citation: Kang, J. E., S. K. Song, H. W. Lee, and Y. K. Kim, 2012: The influence of meteorological conditions and complex topography on ozone concentrations in a valley area near coastal metropolitan cities. Terr. Atmos. Ocean. Sci., 23, 25-38, doi: 10.3319/TAO.2011.06.30.02(A)

1. INTRODUCTION

It is well known that the air quality around urban areas can be greatly affected by emission sources, geographical/topographical features (e.g., coastal and valley areas) and meteorological conditions (e.g., local circulation, transport, and stagnation) within and surrounding these areas. For instance, a maximum ozone (O_3) concentration of ≥ 100 ppb was frequently observed in downwind regions of strong emission sources (e.g., heavy traffic) in California during the summers of 1995 - 1996 (Carroll and Dixon 2002). Within the California South Coast Air Basin (SoCAB), the peak O_3 concentration (about 190 ppb) was shown in a convergence zone where onshore and offshore flows were encountered during a high O_3 episode in August 1997 (Boucouvala and Bornstein 2003; Boucouvala et al. 2003). In addition, the anthropogenic emissions of pollutant gases (e.g., NO_x and VOCs) from industrial facilities in a metropolitan region, Taiwan, were found to contribute to increases in the O_3 concentrations of up to 40 ppb in an urban center adjacent the emission sources and of up to 20 ppb in an inland rural area (about 20 km away from the emission sources), due to the transport of O_3 and its precursors with northerly winds induced by topographical blocking (e.g., high mountains) (Lin et al. 2007).

In recent years, several studies on the contributions of physical (e.g., horizontal and vertical transport) and chemical processes (e.g., chemical production) to the O_3 concentrations around urban areas during summer have been reported in the literature (Huang et al. 2005; Arteta and Cautenet 2007; Shi et al. 2009; Yu et al. 2009; Khiem et al. 2010; Song et al. 2010b). The production of O_3

* *Corresponding author*
E-mail: kimyk@pusan.ac.kr

in the coastal city of Hong Kong was found to account for about 70% of the total O_3 concentrations due to transport from southern China and about 30% due to local chemical production (Huang et al. 2005). In a coastal city in France during the summers of 2000 - 2001, the change in the O_3 concentration (about 30 ppb h^{-1}) due to chemical production was estimated to be slightly higher than that (about 20 ppb h^{-1}) due to transport, via the development of sea and/or upslope breezes (Arteta and Cautenet 2007). Moreover, the contribution of horizontal transport to daytime O_3 concentrations (11 - 175 ppb h^{-1}) around industrial and residential areas of a coastal city in Korea was estimated to be most dominant (Song et al. 2010b). According to a recent study in Japan, the enhancement of surface O_3 concentrations in Tokyo during the summer of 2005 was found to be largely influenced by the downward transport of O_3-rich air from the upper atmosphere (Khiem et al. 2010).

Although there have been a number of modeling studies regarding O_3 pollution around urban areas, detailed investigations that consider both the horizontal and vertical transport of O_3, as well as the accumulation effect induced by geographical/topographical features (e.g., valley and coastal cities), remain to be performed in Asia. In this study, the impact of meteorological conditions and complex topography on the O_3 concentrations was assessed in a valley city close to coastal metropolitan cities in Korea, which included a specific geographical location (e.g., closed and semi-closed topographies covering mountains, residential and/or industrial areas). For the purpose of this study, the horizontal and vertical distributions of O_3 and wind vectors in and around the valley city were simulated to show the relationship between the meteorological and topographical characteristics and O_3 concentrations during the summer of 2006. The contributions of the physical and chemical processes to the O_3 concentrations were also quantitatively evaluated in the study area using a process analysis (PA) method.

2. STUDY AREA, DATA, AND METHODS

Yangsan city, the target area in this study, is located approximately 35 km from the southeastern coast of the Korean Peninsula (Fig. 1). This city includes complex terrain with a valley area surrounded by a number of mountains, public buildings, and residential areas (Song et al. 2009; Song et al. 2010a). It also includes a variety of source regions (e.g., industrial complexes) of pollutant gases in the vicinity of the central downtown area (Fig. 1). Meanwhile, the wind conditions in the study area (i.e., Yangsan) are characterized by two prevailing winds along the central roads in the valley area (Fig. 1); northeasterly and southwesterly winds are fairly dominant across all seasons. Based on the two dominant wind patterns, the air quality in Yangsan can be affected by the transport of pollutant gases (e.g., NO_x and VOCs) due to its location downwind of coastal metropolitan cities, such as Busan (about 15 km south of Yangsan) and Ulsan (30 km northeast of Yangsan), which have large emission sources (e.g., intensive traffic activities, industrial facilities, and shipping). Recently, the significance of ship emissions in O_3 production has been reported with regard to their impact on O_3 concentration (the increase of up to 15 ppb) in the downwind regions of ports in Busan (Song et al. 2010b). During recent years (2006 - 2009), high O_3 days (i.e., days when the average O_3 concentration in an 8 h period exceeds 60 ppb) have frequently been observed in Yangsan (about 50 days y^{-1}), which were similar to those in surrounding coastal areas (e.g., Busan and Ulsan).

To evaluate the influences of meteorological conditions and complex topography on O_3 concentrations in the study area, numerical modeling was applied to high O_3 episodic days during the summer of 2006 (8 and 10 August). A high O_3 concentration of ≥ 100 ppb (up to 150 ppb) was observed in the study area during the episodic days. In addition, to quantify the contributions of the physical and chemical processes to the O_3 concentrations within the mixed layer of the study area, the PA method [the integrated process rate (IPR) and integrated reaction rate (IRR) analyses] was applied during the study period. The IPR and IRR analyses of O_3 provided the rates of each physico-chemical process (e.g., advection, diffusion, deposition and chemistry) and the rates of the integral of the individual chemical reaction for the selected grid cells, respectively (Gipson 1999; also see http://www.epa.gov/asmdnerl/CMAQ/CMAQscienceDoc.html).

For the purposes of this study, two air quality and two meteorological monitoring sites were selected. The two air quality monitoring sites included Jung Ang (JA), located in an urban center area (with a population of about 120 thousand), and Seo Chang (SC), located in a suburban area (with a population of about 45 thousand) in Yangsan (Fig. 1). The JA site was characterized by a semi-closed topography that covers a number of industrial facilities, buildings and high mountains (with heights of ≥ 0.9 km) on the eastern and western sides; the SC site was located within a closed topography, encompassed by a number of low mountains (0.2 - 0.9 km) and residential areas in all directions. In addition, the two meteorological monitoring sites were located less than 1.0 km from air quality monitoring sites. With respect to the meteorological conditions during the episodic days, a high-pressure system passed through the entire study area from east to west (not shown). Due to the movement pattern of the high-pressure system, there were distinct differences in the wind speeds and directions between the JA and SC sites of Yangsan during the study period. For instance, southerly or southeasterly winds at site JA and easterly or northeasterly winds at site SC on 8 August were observed to be dominant; whereas, southerly or southwesterly winds at both sites on 10 August were predominant. This suggests that the extent of air pollution (including O_3) resulting from

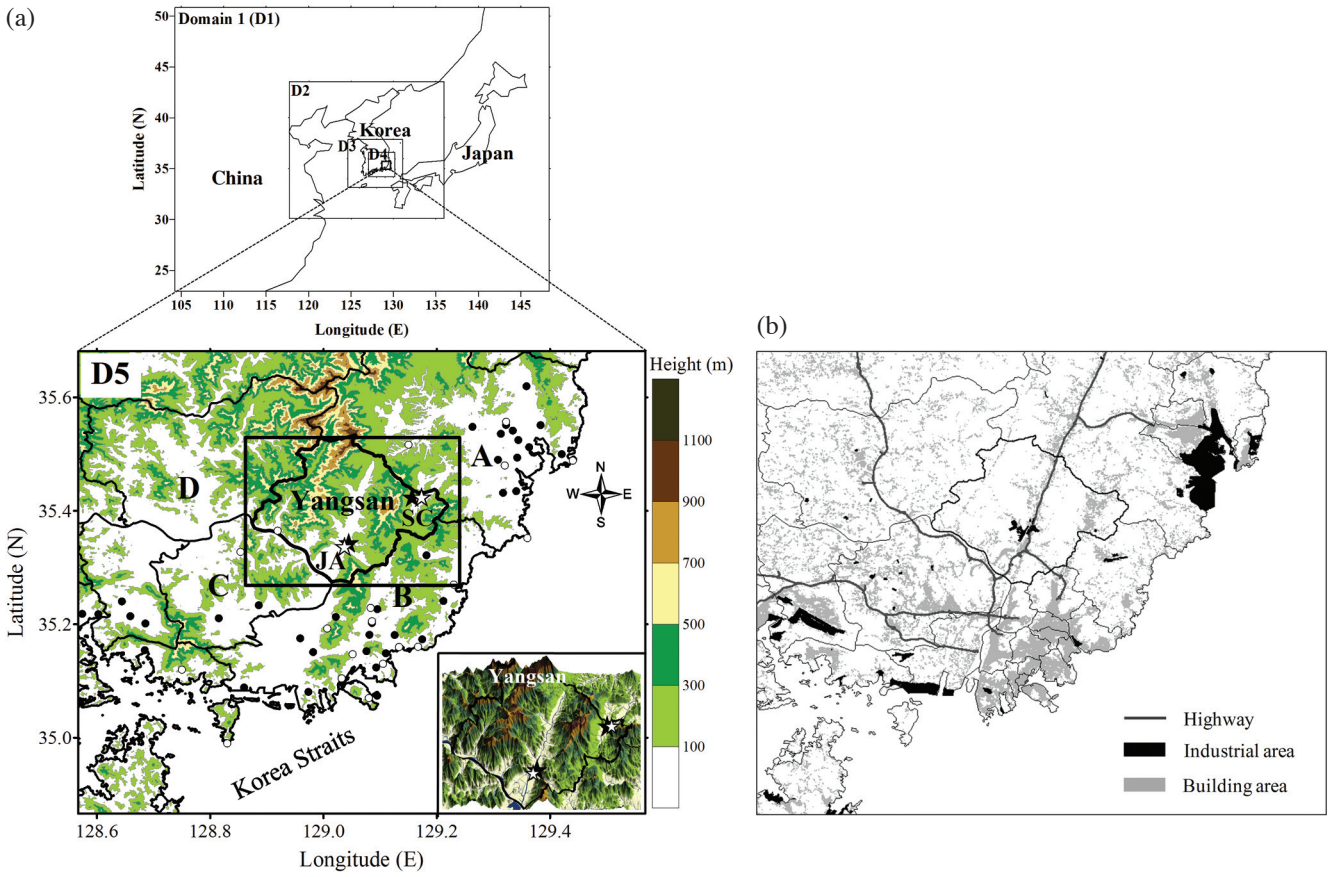

Fig. 1. Map showing (a) the five nested grid domains (Domains 1 - 5) for the MM5 modeling, with a precise topography and (b) land-use types (highway, industrial and building areas) of the target area (Yangsan) in the smallest domain (D5). Legends, air pollutant (●) and meteorological variable (○), in the figure indicate the observation sites. "JA" and "SC" in the figure represent the air quality monitoring sites in Yangsan: Jung Ang (JA) site located in an urban center area and Seo Chang (SC) site located in a suburban area.

the different wind patterns between the two sites and between the two episodic days will be different.

3. MODEL DESCRIPTIONS AND INPUT DATA

The models employed in this study were the PSU/NCAR non-hydrostatic meteorological model (i.e., MM5, Grell et al. 1994) and Model-3/Community Multiscale Air Quality (CMAQ) model (Byun and Schere 2006). The CMAQ, a comprehensive Eulerian photochemical modeling system developed by the US EPA, was configured with the Carbon Bond (CB)-IV chemical mechanism and Meteorology-Chemistry Interface Processor (MCIP) and simulates all atmospheric and land processes that affect the transport, transformation and deposition of atmospheric pollutants, and/or their precursors, on both regional and urban scales. Detailed information regarding the specific processes of the CMAQ modeling system has been described in Byun and Schere (2006).

The MM5 model was used as the meteorological driver for the CMAQ modeling system. The computation domain in the MM5 consisted of 41 sigma vertical layers with the lowest level being 7 m (sigma = 0.999). The model was run on the five grids in the one-way nesting mode (Fig. 1): (1) a coarse grid domain that covers Northeast Asia [domain 1 (D1), 81 km grids, 40 × 38 array], (2) a regional domain (D2, 27 km, 55 × 55), (3) an intermediate regional domain (D3, 9 km, 64 × 58), (4) a small regional domain (D4, 3 km, 91 × 88), and (5) a fine grid domain that covers the study area (i.e., Yangsan) and its surroundings (D5, 1 km, 88 × 88). On the other hand, the CMAQ model was run on two nested grid domains because this study focused on the increase or decrease of O_3 concentration due to the transport and photochemistry of its precursors emitted from regional- or urban-scale environments (e.g., the target area and neighboring coastal cities). The coarse and fine domains of the CMAQ model have 81 × 78 grid points with 3 km resolution (i.e., the fourth domain of the MM5 simulation) and 78 × 78 grid points with 1 km resolution (i.e., the fifth domain of the MM5 simulation), respectively. There were 24 vertical layers from the surface (15 m) to 15 km.

The physical options used for the MM5 simulation were the Grell cumulus parameterization scheme (for D1 and D2), the MRF planetary boundary layer scheme, the Mixed-phase

moisture scheme, the RRTM radiation scheme, and the Noah Land-Surface Model. The MM5 simulations were carried out using the 23-category land-use data (a 90-m resolution) from the Environmental Geographic Information System (EGIS) (http://egis.me.go.kr/egis/) to more effectively reflect surface conditions (especially for the 'urban' classification for D4 and D5) of the study area. The initial and boundary conditions in the MM5 simulations were generated every 6 h by interpolating the National Center for Environmental Prediction (NCEP)-FNL analysis fields, with a 1-degree resolution, at standard pressure levels. A time step of 2 s was employed for a 120-h period (from 0000 Universal Time Coordinated (UTC) on 6 August to 0000 UTC on 11 August 2006). Meanwhile, for the CMAQ simulations, the initial and boundary conditions for the surface O_3 and its precursors in the coarse domain (3 km grids) were derived from surface background data observed at the respective monitoring sites closest to the four boundaries within the model domain. In addition, the initial and boundary conditions for the O_3 in the upper layer were obtained from the O_3 sounding data at an upper air observatory [the only ozonesonde station (in Korea) located at northeast from the target area] due to the restrictions in field observations.

For the CMAQ simulation, the land-based emission rates of pollutant gases (e.g., NO_x and VOCs) in the study domain were estimated using the Clean Air Policy Support System (CAPSS) provided by the National Institute of Environmental Research (NIER), Korea. Moreover, based on the Emissions Modeling Clearinghouse (EMCH), both the temporal and spatial allocation of these emissions, as well as the split factors for chemical speciation, were considered for the simulations (http://www.epa.gov/ttn/chief/emch/). In this study, the emission rates of the pollutant gases from ships were used also to consider their impact on the O_3 concentrations in the target area. A detailed description on emissions from ships traversing ports in Busan was given in Song et al. (2010b). In brief, the ship emissions (g h^{-1}) were calculated using the maximum continuous rated engine power (kW), the load factor (%) for propulsion, auxiliary, and harbor craft engines, the actual activity (hours), and the power-based emission factor (g kW^{-1} h^{-1}) (CARB 2006; Starcrest Consulting Group, LLC 2009). The spatial distributions of the emissions of NO_x and VOCs (kg day^{-1}) in the model domain are given in Fig. 2. The emissions of NO_x and VOCs were mostly concentrated around the anthropogenic source regions (e.g., industrial areas, roads, and/or ports) of Busan and Ulsan, while; in part, being distributed along the valley area (covering a number of industrial facilities, roads and buildings) of Yangsan (Fig. 1).

4. RESULTS AND DISCUSSION

4.1 The Role of Meteorological Conditions and Complex Topography on O_3 Distributions

The impact of meteorological conditions and complex topography on O_3 concentrations were assessed by analyzing the differences in the temporal and spatial distributions of O_3 between sites JA and SC in the valley area using the MM5-CMAQ modeling system. For the purpose of this study, a 24-h simulation run of the surface O_3 concentrations and wind fields was conducted during the entire study period (8 - 10 August 2006). During the length of simulation period, the horizontal distributions of O_3 and wind vectors at two different time bands [1200 and 1600 local standard time (LST)] on both 8 and 10 August were analyzed for comparison (Fig. 3). Overall, the O_3 concentrations at the surface level depended largely on the wind direction and speed of the air inflow with respect to the specific topographical features (e.g., closed and semi-closed topographies). On 8 August, the highest O_3 concentration (up to 130 ppb) at 1200 LST was predicted in the southwestern part of the model domain (e.g., downwind locations of source regions of Busan,

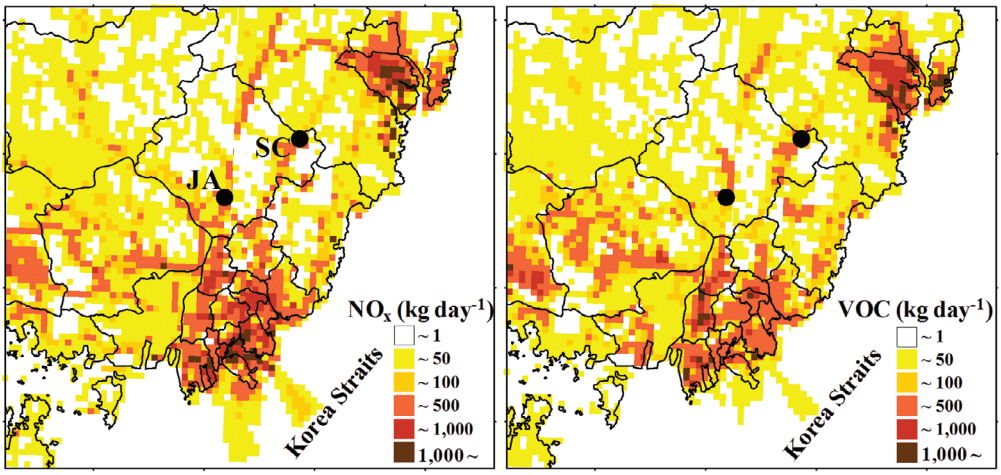

Fig. 2. The spatial distributions of the emissions of NO_x and VOCs in the study domain (in kg day^{-1}).

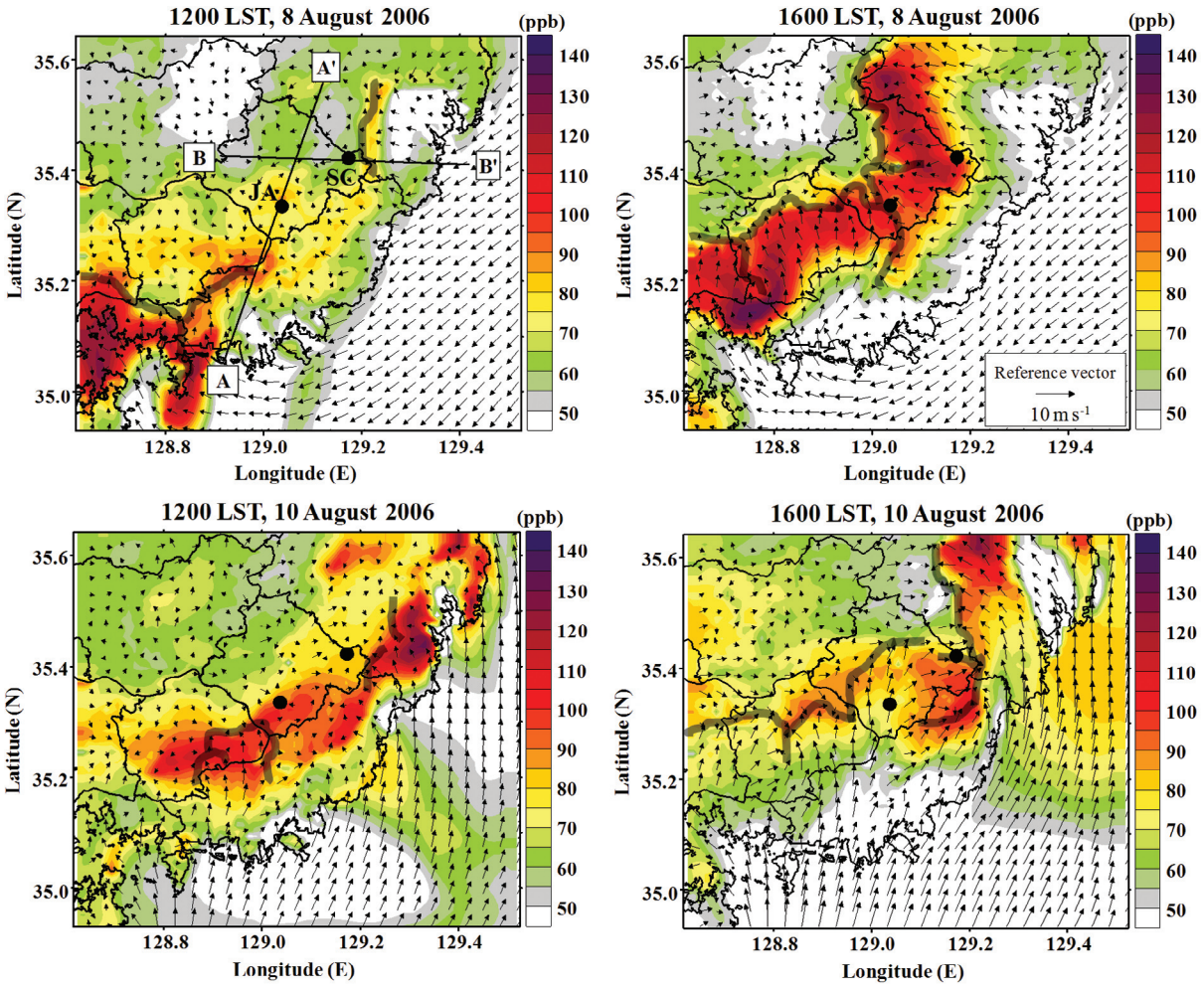

Fig. 3. Horizontal distributions of the simulated O_3 concentrations (ppb) and wind vectors (m s^{-1}) at 1200 and 1600 LST during the episodic days (8 and 10 August 2006). The thick lines indicate the wind convergence zones. A - A' and B - B' denote the vertical cross-section lines.

as shown in Fig. 2) due to the combination of both an easterly sea breeze and its convergence caused by topographical blocking (e.g., mountains) (Figs. 1 and 3). After four hours (1600 LST), the region of highest O_3 concentration extended to the central part of the model domain (e.g., Gimhae and Yangsan) due to the rapid transport with southerly and/or easterly winds (e.g., ≥ 5 m s^{-1}).

The O_3 concentrations (90 - 110 ppb) around the valley area, including sites JA and SC (i.e., the downwind areas of Busan and Ulsan, respectively), at 1600 LST on 8 August were considerably higher than those (60 - 80 ppb) at 1200 LST on the same day. The high O_3 concentration at JA site at 1600 LST was found to be due to the combined effects of both the transport of O_3 and its precursors and their subsequent reaction from the source regions of Busan (with a southerly or southeasterly sea breeze, Figs. 3 and 4) and Ulsan (with a easterly sea breeze, Fig. 3), as well as their accumulation in a convergence zone (located within the valley topography), where these wind systems converged. This trend was in qualitative agreement with previous studies (Lu and Turco 1995; Liu and Chan 2002; Huang et al. 2005). Unlike the JA site, the elevated O_3 level at the SC site at 1600 LST on 8 August might have been caused primarily by the transport of O_3 and its precursors and their subsequent reaction from the source regions of Ulsan with the strong easterly and northeasterly wind (Figs. 3 and 4). On the other hand, relatively low O_3 concentrations of ≤ 50 ppb were predicted to occur around the coastal areas of both Busan and Ulsan due to the significantly large NO_x emissions (e.g., a maximum of ≥ 1000 kg day^{-1}, as shown in Fig. 2), causing an enhanced NO_x removal.

The temporal and spatial distributions of O_3 simulated on 10 August were distinguishable from those on 8 August. On 10 August, the highest O_3 concentration (≥ 100 ppb) at 1200 LST was predicted to occur around the downwind areas (i.e., northern locations) of Busan and/or Ulsan (e.g., the convergence zone located around inland mountains and valleys, as shown in Fig. 1), due to transport from the coast to inland locations with the southerly sea breeze. In addition, at the same time, the O_3 concentration (about 90 ppb) at JA

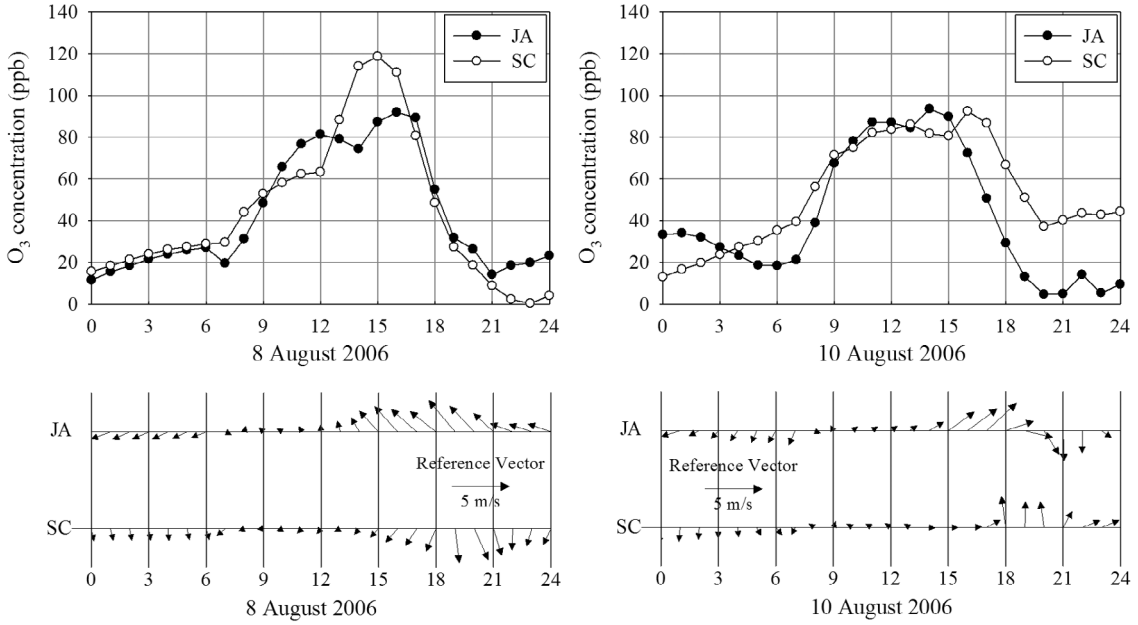

Fig. 4. Diurnal variations of the simulated O_3 concentrations (ppb) and wind vectors (m s^{-1}) at sites JA and SC during the episodic days (8 and 10 August 2006).

site (within the semi-closed topography) was slightly higher than that (80 ppb) at SC site (within the closed topography). The relatively high O_3 concentration at the JA site may possibly have been due to the accumulation of O_3 and its precursors and their subsequent reaction (from local emission sources) as a result of the weakness of the wind speed (1 - 2 m s^{-1}). Conversely, the O_3 concentration (about 90 ppb) at 1600 LST was significantly higher at the SC site than that (70 ppb) at the JA site. The difference between the two sites might have been caused mainly by the effective dilution at the JA site due to a strong southerly or southwesterly sea breeze, at approximately 6 m s^{-1} (rather than SC site) and; in part, by the inflow of O_3 itself to SC site with the change (southerly or southwesterly to westerly winds) in the wind direction of the strong sea breeze (Figs. 3 and 4).

For a detailed comparison between the vertical distributions of O_3 and wind vectors at 1200 and 1600 LST on the two episodic days (8 and 10 August), the vertical cross sections of O_3, potential temperature and wind vectors at and around sites JA and SC (Fig. 5) were analyzed as well. Two vertical cross section lines, A to A' for JA site and B to B' for SC site, are shown in Fig. 3. On 8 August, high levels of O_3 (≥ 90 ppb) at 1200 LST were mixed from the surface to the top (about 1 km) of the boundary layer over a region located at about 20 km south from JA site, where the vertical gradient of the potential temperature was very weak (Fig. 5a). At 1600 LST, the O_3-rich air arrived near JA site (within 1 km south of JA) due to the penetration of the southerly sea breeze. On the other hand, the vertical up-mixing of O_3 was predicted to occur at the JA site, from the surface to 1.7 km, due to the upward motion in the convergence zone, where the southerly and northeasterly (shifted from the easterly sea breeze) winds converged (Figs. 3 and 5a). At the SC site, the inflow of high O_3 levels (90 - 120 ppb) was predicted to occur at 1600 LST due to the horizontal flows within the elevations (about 0.5 km) of the valley topography with the easterly sea breeze, but such a phenomenon was not apparent at 1200 LST (Figs. 3 and 5a). In addition, the layer of high O_3 concentrations (about 1.0 km) at SC site at 1600 LST was considerably lower than that (about 1.7 km) at JA site for the same time, possibly due to differences in the geophysical/topographical features (e.g., closed and semi-closed topographies) and the direction of the movement of the sea breezes to the two sites.

On 10 August, the southerly sea breeze with high O_3 levels was observed outside the JA site at 1200 LST, and during the next four hours (1600 LST), the O_3-rich air was rapidly funneled into the JA site (within the semi-closed topography, as shown in Fig. 1) with the strong sea breeze; whereas, the easterly sea breeze with high O_3 levels observed outside the SC site (at 1200 LST) did not penetrate this site at 1600 LST (Figs. 3 and 5b). Although there was no penetration of the easterly sea breeze (including the high O_3 levels) at the SC site, the O_3 concentrations (90 - 100 ppb) at this site were considerably higher than those (70 - 85 ppb) at the JA site. This might have been caused mainly by the downslope flows from the top of the western mountains (about 0.9 km) with the change (southerly or southwesterly to westerly winds) in the sea breeze (Figs. 3 and 5b). On the other hand, at the JA site, the O_3 concentrations (≤ 85 ppb) with weak vertical mixing (surface to 0.6 km) at 1600 LST on 10 August were considerably lower than those (≥ 100 ppb)

with strong vertical mixing (surface to 1.7 km) for the same time on 8 August. Despite the low mixing heights at JA site on 10 August, the relatively low O_3 concentrations at this site were likely to be due to a dilution effect induced by the strong southerly sea breeze.

4.2 Process Analysis at the Selected Sites in the Valley Area

Figure 6 shows the relative changes in the mean O_3 concentrations calculated from the IPR analysis at the surface levels of two different sites (JA and SC) within the study area (i.e., Yangsan) during the afternoon periods (1200 through 1700 LST) of the two episodic days (8 and 10 August). Note that the main processes of the IPR include horizontal transport (HTRA: the sum of horizontal advection and diffusion), vertical transport (ZTRA: the sum of vertical advection and diffusion), dry deposition (DDEP) and gas-phase chemical production/destruction (CHEM), which lead to changes in the O_3 concentrations. On 8 August, the HTRA at the JA and SC sites was the main contributor to the O_3 concentrations/production. For example, the changes in the O_3 concentrations due to the HTRA were predicted to be about 240 and 120 ppb h^{-1} at sites JA and SC, respectively. Therefore, substantial contributions of the HTRA at both sites led to the high O_3 concentrations at these sites, as shown in Fig. 3. On the other hand, O_3 concentrations of about 180 (JA site) and 140 ppb h^{-1} (SC site) at the two sites were largely removed by the ZTRA. The relatively large O_3 loss at the JA site might have been primarily caused by the upward motion in the convergence zone under specific meteorological (e.g., wind convergence) and topographical conditions at this site (e.g., the semi-closed topography) (Figs. 3 and 5).

The production or loss of O_3 due to individual processes on 8 August was distinguishable from that on 10 August. On 10 August, the ZTRA was the main contributor to the production of O_3, regardless of the sites. For instance, the changes in O_3 concentrations due to the ZTRA were predicted to be about 110 and 190 ppb h^{-1} at sites JA and SC, respectively. In particular, the O_3 production due to the ZTRA at site SC was significantly (an order of magnitude) higher than that ($\leq$ 10 ppb h^{-1}) due to the CHEM at this site. The relatively large O_3 production at the SC site was largely related to the vertical inflow of wind from the top of the western mountains at this site, as shown in Fig. 5. On the other hand, the DDEP (about 60 ppb h^{-1}) at the JA site and the HTRA (180 ppb h^{-1}) at the SC site largely contributed to the losses of O_3. Such losses of O_3 due to the HTRA at the SC site were significantly (a factor of 4) larger than those ($\leq$ 40 ppb h^{-1}) at the JA site. The larger losses at SC site were likely to be related to the divergence at low levels in order to balance the downward motion from the top region of the valley (including this site) due to the ZTRA (Wang et al. 2010).

Based on the above IPR analysis, the effects of the HTRA and ZTRA were estimated to be highest on the production or loss of O_3 at both sites during the study period. For a detailed analysis with respect to their effect at both sites, the contributions (%) of horizontal advection in the east-west (i.e., XADV) and north-south directions (i.e., YADV) and vertical advection (i.e., ZADV) to the O_3 concentrations with height have been discussed for the afternoon periods of 8 and 10 August (Fig. 7). Moreover, the contributions of the other two processes (e.g., DDEP and CHEM) with height were also discussed for comparison. Note that the positive values for the XADV, YADV, and ZADV indicate the contributions of their respective O_3 productions to the total O_3 production (i.e., O_3 inflow), while negative values denote the contributions of their respective O_3 losses to the total O_3 loss (i.e., O_3 outflow).

On 8 August, the XADV (a mean of 59%) and YADV (56%) were the main contributors to the production of O_3 in the lower layers at the sites SC (surface to about 0.5 km) and JA (surface to 0.9 km), respectively, while the O_3 losses in the lower layers at the sites SC (surface to 0.43 km) and JA (surface to 0.7 km) were most significantly affected by the ZADV (-90%), and vice versa for the most upper layers (Fig. 7). In addition, the height of the maximum O_3 inflow (about 0.6 km) due to horizontal advection at the JA site was found to be somewhat higher than that (about 0.4 km) at the SC site, due to the different heights of the mountains within the valley topography (Fig. 1). At the heights of maximum O_3 inflows to the two sites, the increases in the contributions of the CHEM might be closely related to the photochemical reactions of O_3 with its precursors during the horizontal advection at these heights (Fig. 7). These maxima O_3 inflows at these heights for both sites led to the higher concentrations of vertical O_3 at similar heights, as shown in Fig. 5a. Subsequently, this estimation suggests that the high O_3 concentrations at both sites were mainly affected by the transport of O_3 and its precursors from the source regions; Busan for JA site (e.g., the large contribution of YADV) and Ulsan for SC site (e.g., the large contribution of XADV).

The contributions of the individual physical and chemical processes to the productions or losses of O_3 at the two sites on 10 August were distinguishable from those on 8 August. On 10 August, the large O_3 outflows (means of -73% and -96% at sites JA and SC, respectively) due to the XADV were predicted to occur at heights below 1 km at both sites. The O_3 inflows (means of $\leq$ 40%) due to the YADV from the source regions of Busan were predicted to occur in the lower layer at the JA site (at heights below 0.5 km) and throughout the entire layer (especially around the top regions of mountains) at the SC site. Here, the O_3 inflow due to the YADV at the SC site might directly induce the downward transport of O_3 to the lower layer (including the surface) at this site. Therefore, the contribution of the ZADV (approximately 83%) near the surface level at the

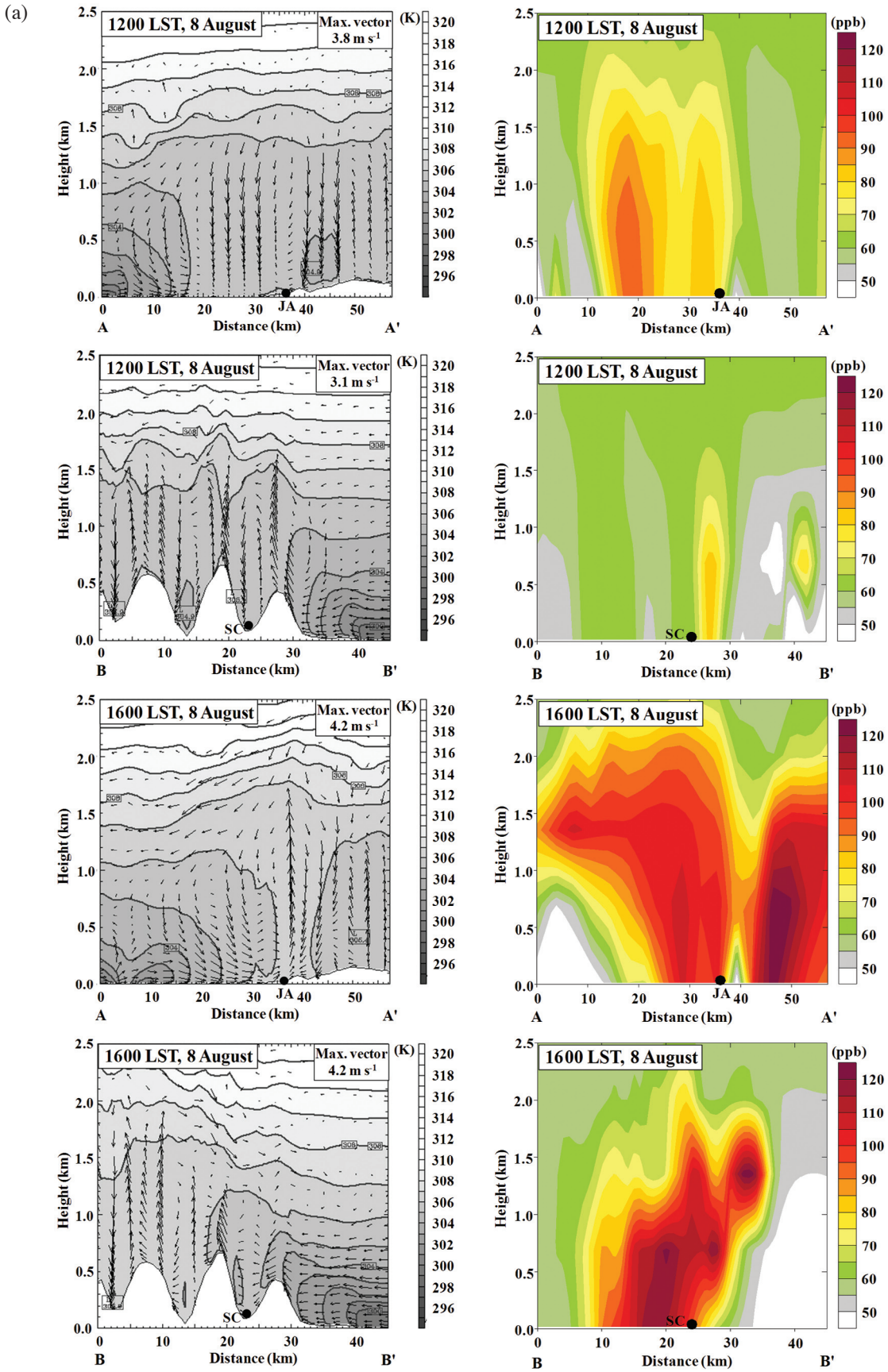

Fig. 5. Vertical cross sections of the potential temperatures (K, solid lines), wind vectors (m s^{-1}, arrows) and O_3 concentrations (ppb, contours) at 1200 and 1600 LST on (a) 8 and (b) 10 August 2006, along lines A - A' (for site JA) and B - B' (for site SC), as shown in Fig. 3.

(b)

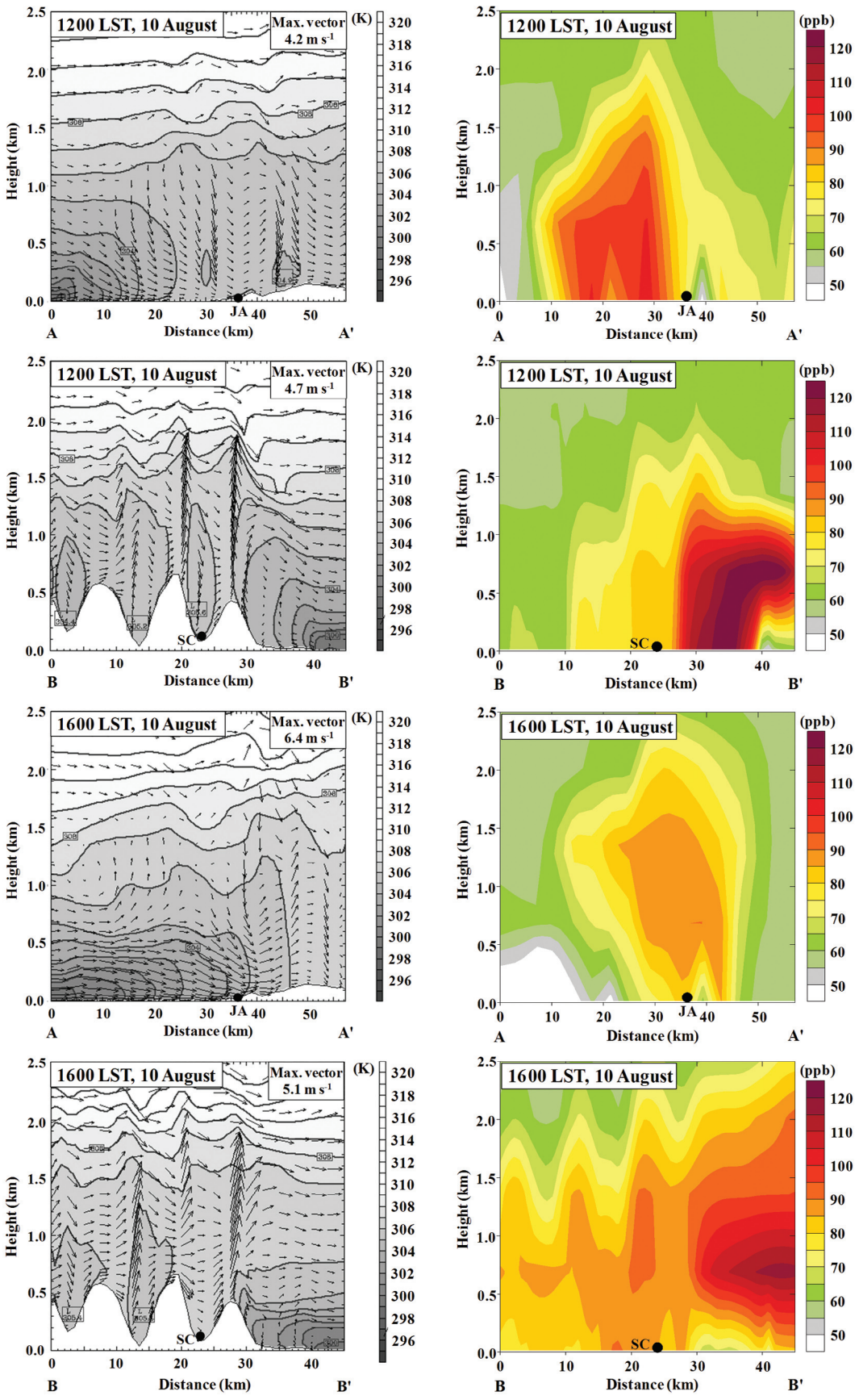

Fig. 5. (Continued)

SC site was found to be significantly (a factor of 3.5) higher than that (24%) at the JA site, causing higher O_3 concentrations within the mixed layer (including the surface) at the SC site (Fig. 5b). In addition, the largest O_3 inflows due to the YADV were predicted at heights of about 0.15 and 0.9 km at the JA and SC sites, respectively, due to the difference in the mixed-layer heights induced by the different intensities of the sea breezes between the two sites. On the other hand, the CHEM and DDEP at the two sites on the two episodic days (8 and 10 August 2006) were relatively minor contributors to the production/destruction of O_3, compared to the other processes (Fig. 7). In brief, the results derived at the two sites during the study period might have been caused by the different meteorological conditions (e.g., the movement direction and intensity of sea breezes) and topographical features (e.g., the semi-closed topography at the JA site and the closed topography at the SC site) between the two sites.

Table 1 provides a comparison of the IRR analyses related to the production/destruction of O_3 at both the surface and height of maximum O_3 inflow between the JA and SC sites at 1200 and 1600 LST on the two episodic days (8 and 10 August 2006). On both 8 and 10 August, the rates of photochemical O_3 production [$P(O_3)$, P1 + P2] at the surface level of the two sites at 1200 LST were mostly higher than those at 1600 LST, possibly because of the accumulation of O_3 and its precursors due to the very weak winds (about 1 m s^{-1}, as shown in Fig. 4). Despite the higher $P(O_3)$ at 1200 LST, the O_3 concentrations at this time were lower than those at 1600 LST (Figs. 3 and 4). This might have been due to the transport of O_3 and its precursors from the local or coastal emission sources rather than the contribution of their photochemistry. As for the IRR analyses of O_3 at the heights of maximum O_3 inflow, the $P(O_3)$ values at both sites were slightly different between 8 and 10 August. For instance, at 1600 LST on 8 August, the $P(O_3)$ (21 ppb h^{-1}) at the height (about 0.4 km) of maximum O_3 inflow at site SC was significantly (a factor of about 2) higher than that (10 ppb h^{-1}) at (about 0.6 km) the JA site, and vice versa for 10 August. The relatively higher $P(O_3)$ at SC site was likely to imply the larger photochemical production of O_3 during the horizontal transport. On the other hand, the rates of photochemical O_3 destruction [$D(O_3)$, P3 + P4 + P5], the NO_x loss, and termination rates of HO_2 and RO_2 at the two levels at both sites during the study period were significantly low.

5. MODEL VALIDATION

To assess the agreement between the observed and predicted values of the meteorological variables (air temperature and wind speed) and the O_3 concentrations, statistical analyses were conducted at several monitoring sites (24 sites for meteorological variables and 37 sites for O_3, Fig. 1), including the JA and SC sites, during the entire simulation period (8 - 10 August 2006) (Table 2). For model computation, the basic statistical parameters [mean, standard deviation, root mean square error (RMSE) and index of agreement (IOA)] were derived for both the observed and predicted data sets. In addition, the mean normalized bias error (MNBE), mean normalized gross error (MNGE), and unpaired peak prediction accuracy (UPA), which are commonly used to evaluate the model performance of O_3 in regions where monitoring data are sufficiently dense, were calculated (US EPA 1991). The criteria values for the MNBE, MNGE, and UPA ranged from ±5 to ±15, 30 to 35, and ±15 to ±20%, respectively (US EPA 1991). Note that the observation-prediction pairs of the O_3 concentration, if observed to be below 60 ppb, were excluded from the statistical analyses (Russell and Dennis 2000; Hogrefe et al. 2001; Tsai and Wu 2006).

As shown in Table 2, the IOAs of air temperatures, wind speeds, and O_3 concentrations were generally calculated to be more than 0.6 at most of the monitoring sites, with their maximum IOAs of 0.94 (SC site), 0.63 (JA site), and 0.82 (JA site), respectively. The RMSEs of the two meteorological variables were less than 2.3°C and 1.6 m s^{-1} for the air temperature and wind speed, respectively. In addition,

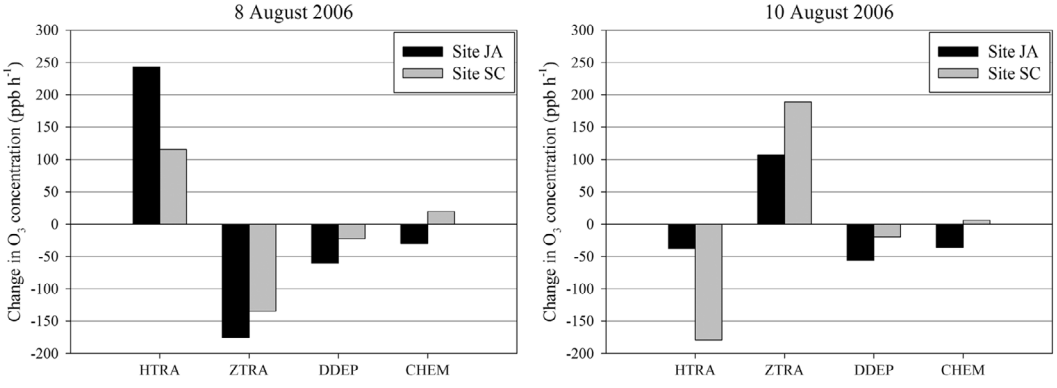

Fig. 6. Comparison of the integrated process rates (IPR) (ppb h^{-1}) of O_3 at the surface levels of sites JA and SC during the afternoon periods (1200 to 1700 LST) of the two episodic days (8 and 10 August 2006).

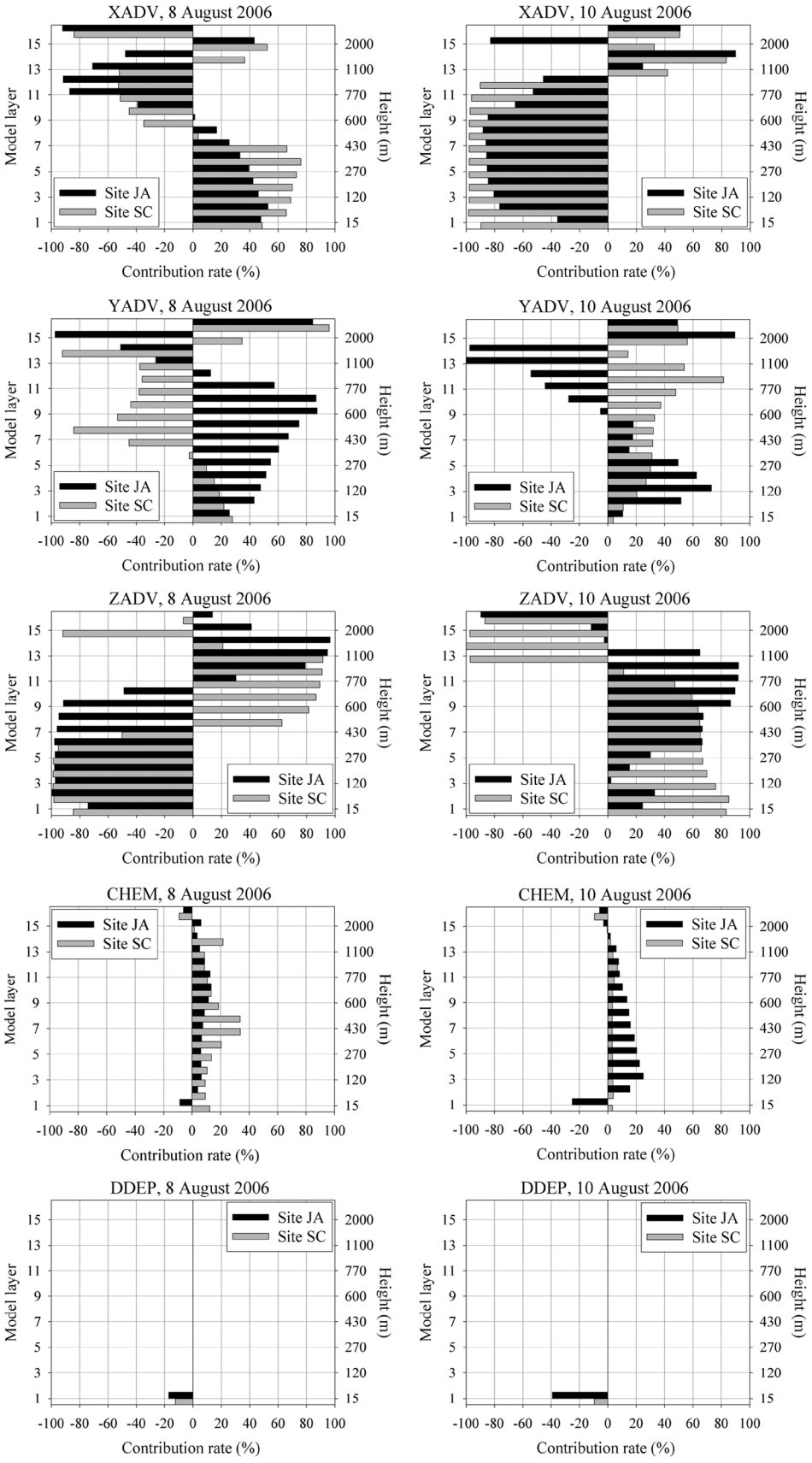

Fig. 7. Relative contributions (%) of horizontal (i.e., XADV and YADV) and vertical advection (i.e., ZADV), chemical production/destruction (i.e., CHEM), and dry deposition (i.e., DDEP) to the O_3 concentrations with heights calculated from the integrated process rate (IPR) analysis at heights below 2.5 km at sites JA and SC during the afternoon periods (1200 to 1700 LST) of the two episodic days (8 and 10 August 2006).

Table 1. Comparisons of the integrated reaction rate (IRR) (ppb h^{-1}) related to O_3 production/destruction at (a) the surface and (b) heights of maximum O_3 inflow between sites JA and SC at 1200 and 1600 LST on 8 and 10 August 2006.

[A] The surface level

Category*		Reactants	8 August				10 August			
			1200 LST		1600 LST		1200 LST		1600 LST	
			JA	SC	JA	SC	JA	SC	JA	SC
$P(O_3)$	P1	$HO_2 + NO$	27.42	11.10	23.08	13.60	27.13	9.18	7.65	6.42
	P2	$RO_2 + NO$	27.38	13.36	25.80	13.42	25.50	13.52	7.10	9.34
All			54.80	24.46	48.88	27.02	52.63	22.70	14.75	15.76
$D(O_3)$	P3	$O(^1D) + H_2O$	1.64	1.48	0.50	0.52	1.86	1.87	0.35	0.38
	P4	$O_3 + OH$	0.31	0.18	0.13	0.12	0.40	0.17	0.09	0.05
	P5	$O_3 + HO_2$	0.47	0.71	0.39	0.42	0.55	1.07	0.07	0.67
All			2.42	2.37	1.02	1.06	2.81	3.11	0.51	1.10
$N(O_3)$			52.40	22.10	47.87	25.97	49.81	19.58	14.23	14.66
NO_x loss	P6	$NO_2 + OH$	3.68	0.70	2.20	1.44	3.49	0.42	2.04	0.22
HO_2 termination	P7	$HO_2 + HO_2$	0.21	0.67	0.11	0.13	0.31	1.07	0.01	0.37
RO_2 termination	P8	$RO_2 + RO_2$	0.05	0.24	0.04	0.04	0.07	0.52	0.00	0.23
	P9	$RO_2 + HO_2$	0.39	1.49	0.24	0.25	0.54	2.84	0.01	1.02

[B] The heights of maximum O_3 inflow**

$P(O_3)$	P1	$HO_2 + NO$	11.70	7.33	4.14	10.91	12.30	2.13	5.75	1.94
	P2	$RO_2 + NO$	12.13	8.73	5.71	10.33	13.37	3.90	5.10	2.94
All			23.83	16.06	9.85	21.24	25.67	6.03	10.85	4.88
$D(O_3)$	P3	$O(^1D) + H_2O$	1.83	1.63	0.62	0.60	1.91	2.08	0.39	0.46
	P4	$O_3 + OH$	0.18	0.14	0.06	0.10	0.27	0.09	0.11	0.03
	P5	$O_3 + HO_2$	0.71	0.67	0.75	0.43	0.88	0.79	0.19	0.49
All			2.72	2.44	1.43	1.13	3.06	2.96	0.69	0.98
$N(O_3)$			21.10	13.62	8.42	20.11	22.61	3.06	10.17	3.89
NO_x loss	P6	$NO_2 + OH$	0.82	0.42	0.16	0.97	1.00	0.07	1.14	0.06
HO_2 termination	P7	$HO_2 + HO_2$	0.58	0.66	0.41	0.15	0.79	0.84	0.05	0.26
RO_2 termination	P8	$RO_2 + RO_2$	0.18	0.27	0.21	0.04	0.22	0.63	0.01	0.18
	P9	$RO_2 + HO_2$	1.14	1.53	1.07	0.28	1.56	2.79	0.08	0.75

** $P(O_3)$: the rate of photochemical O_3 production; $D(O_3)$: the rate of photochemical O_3 destruction; $N(O_3)$: the net photochemical production rate of O_3 (ppb h^{-1}) [=$P(O_3)$ - $D(O_3)$].*

*** The heights of maximum O_3 inflow in the part [B] represent about 0.6 (JA) and 0.4 km (SC) on 8 August and 0.15 (JA) and 0.9 km (SC) on 10 August, respectively.*

Table 2. Statistical evaluation of the meteorological variables and O_3 concentrations between the observed and model-predicted values: results compared at several monitoring sites ("All", 24 sites for meteorological variables and 37 sites for O_3, Fig. 1), including sites JA and SC, during the entire simulation period (8 - 10 August 2006).

Category*	Air temperature			Wind speed			O_3		
	All	JA	SC	All	JA	SC	All	JA	SC
RMSE	2.327	1.855	1.771	1.467	1.615	1.092	23.233	24.264	28.585
IOA	0.849	0.918	0.936	0.613	0.631	0.533	0.780	0.821	0.777
MNBE	-	-	-	-	-	-	-13.004	-11.554	-11.781
MNGE	-	-	-	-	-	-	29.759	20.065	26.234
UPA	-	-	-	-	-	-	-11.316	-3.676	-14.387

** RMSE: root mean square error; IOA: index of agreement; MNBE: mean normalized bias error; MNGE: mean normalized gross error; UPA: unpaired peak prediction accuracy.*

the MNBE (-13.0%), MNGE (29.8%), and UPA (-11.3%) of the O_3 concentrations were calculated to be less than their criteria values (±5 - ±15, 30 - 35, and ±15 - ±20% for the MNBE, MNGE, and UPA, respectively) at several monitoring sites, including the JA and SC sites.

The IOA and RMSE for the meteorological variables, and the MNBE, MNGE and UPA for O_3 calculated in this study were similar to those reported in the literature associated with other applications of meteorological (e.g., MM5) and air quality models (e.g., CMAQ) for complex terrain. Previous studies found IOAs for the wind speed and air temperature ranging from 0.40 to 0.60 (Shi et al. 2009) and 0.68 to 0.89 (Song et al. 2010a), respectively. The RMSEs for the wind speed and air temperature ranged from 1.80 to 2.30 m s^{-1} (Shi et al. 2009) and 2.75 to 3.45°C (Song et al. 2010a), respectively. In addition, the MNBE, MNGE, and UPA for O_3 ranged from -14.3 to -2.1%, 16.8 to 26.7%, and -11.7 to 14.4%, respectively (Jiménez et al. 2005, 2006). Therefore, the statistical analyses undertaken in this study indicated that the model simulation might be reasonable for assessing the influences of the meteorological conditions and topographical features on the O_3 concentrations in the study area.

6. SUMMARY AND CONCLUSIONS

The impact of the meteorological conditions and complex topography on O_3 concentrations in the valley city (Yangsan), including the two different sites (JA and SC), were evaluated during the O_3 episodic days (8 and 10 August) based on a numerical modeling approach (i.e., the MM5-CMAQ modeling system). The PA (IPR and IRR analyses) was employed to compare the contributions of the physical and chemical processes to the O_3 concentrations (within the mixed layer) between the two sites during the afternoon periods (1200 - 1700 LST) of the two episodic days.

A high O_3 concentration at the JA site on 8 August was predicted at 1600 LST (rather than 1200 LST). This might have been due to the combined effects of the horizontal transport of O_3 and its precursors and their subsequent reaction (e.g., the photochemical O_3 production of up to 48 ppb h^{-1}) emitted from the source regions with the southerly (from Busan) and easterly sea breezes (from Ulsan), as well as their accumulation in a convergence zone where these wind systems joined in the valley area (e.g., the semi-closed topography). Such a phenomenon at the SC site (especially, 1600 LST) on the same day was found to be mainly due to the transport from the source regions of Ulsan. In contrast, high O_3 concentrations at both sites on 10 August were predicted to occur at different time bands (e.g., 1200 and 1600 LST at sites JA and SC, respectively). The elevated O_3 level at the JA site was caused mainly by the vertical transport (from about 0.15 km) of O_3 and its precursors and in part by their accumulation and photochemistry (e.g., up to 50 ppb h^{-1}) from local emission sources due to weak winds (1 - 2 m s^{-1}), while that at the SC site was due to the transport of downslope flows (e.g., downward transport) from the top of the western mountains with the changed wind systems (southerly or southwesterly to westerly winds) rather than the contribution from the accumulation of local emissions.

From the PA, the most dominant contributor to the O_3 concentrations at both sites on 8 August was found to be the HTRA from the source regions of Busan and/or Ulsan [e.g., the contributions of the YADV (a mean of 56%) for site JA and XADV (59%) for site SC]. In contrast, on 10 August, the ZTRA within the valley topography at both sites [e.g., the contributions of the ZADV (24% and 83% near surface, respectively) at sites JA and SC] largely contributed to the O_3 concentrations, compared to the other processes (e.g., HTRA, CHEM, and DDEP). In addition, the heights of the largest O_3 inflows due to the advection were different between the two sites and between the two episode days, which were strongly dependent on the different heights of the mountains and the different movement directions and/or intensities of the sea breezes between both sites. Therefore, this confirmed that the differences in the O_3 concentrations between the two sites during the study period were greatly affected by the distinctly different meteorological conditions and topographical features (e.g., closed and semi-closed topographies in the valley area) between these sites.

Acknowledgements This work was funded by the Korea Meteorological Administration Research and Development Program under Grant CATER 2009-3308. This research was also supported by Basic Science Research Program through the National Research Foundation of Korea (NRF) funded by the Ministry of Education, Science and Technology (2010-0012045).

REFERENCES

Arteta, J. and S. Cautenet, 2007: Study of ozone distribution over the south-eastern France (ESCOMPTE campaign): discrimination between ozone tendencies due to chemistry and to transport. *J. Atmos. Chem.*, **58**, 111-130, doi: 10.1007/s10874-007-9081-y. [Link]

Boucouvala, D. and R. Bornstein, 2003: Analysis of transport patterns during an SCOS97-NARSTO episode. *Atmos. Environ.*, **37**, 73-94, doi: 10.1016/S1352-2310(03)00383-2. [Link]

Boucouvala, D., R. Bornstein, J. Wilkinson, and D. Miller, 2003: MM5 simulations of a SCOS97-NARSTO episode. *Atmos. Environ.*, **37**, 95-117, doi: 10.1016/S1352-2310(03)00384-4. [Link]

Byun, D. and K. L. Schere, 2006: Review of the governing equations, computational algorithms, and other components of the Models-3 Community Multiscale Air

Quality (CMAQ) modeling system. *Appl. Mech. Rev.*, **59**, 51-77, doi: 10.1115/1.2128636. [Link]

CARB (California Air Resources Board), 2006: Diesel Particulate Matter Exposure Assessment Study for the Ports of Los Angeles and Long Beach, Final Report. 69-70, California Environmental Protection Agency, Air Resources Board.

Carroll, J. J. and A. J. Dixon, 2002: Regional scale transport over complex terrain, a case study: Tracing the Sacramento plume in the Sierra Nevada of California. *Atmos. Environ.*, **36**, 3745-3758, doi: 10.1016/S1352-2310(02)00305-9. [Link]

Gipson, G. L., 1999: Process analysis. In: Byun, D. W. and J. K. S. Ching (Eds.), Science Algorithms of the EPA Models-3 Community Multiscale Air Quality (CMAQ) Modeling System. EPA Report No. EPA/600/R-99/030 (chapter 16).

Grell, G. A., J. Dudhia, and D. R. Stauffer, 1994: A description of the fifth-generation Penn State/NCAR Mesoscale Model (MM5). NCAR Technical Note, TN-398+STR.

Hogrefe, C., S. T. Rao, P. Kasibhatla, W. Hao, G. Sistla, R. Mathur, and J. McHenry, 2001: Evaluating the performance of regional-scale photochemical modeling systems: Part II - ozone predictions. *Atmos. Environ.*, **35**, 4175-4188, doi: 10.1016/S1352-2310(01)00183-2. [Link]

Huang, J. P., J. C. H. Fung, A. K. H. Lau, and Y. Qin, 2005: Numerical simulation and process analysis of typhoon-related ozone episodes in Hong Kong. *J. Geophys. Res.*, **110**, D05301, doi: 10.1029/2004JD004914. [Link]

Jiménez, P., R. Parra, S. Gassó, and J. M. Baldasano, 2005: Modeling the ozone weekend effect in very complex terrains: A case study in the northeastern Iberian Peninsula. *Atmos. Environ.*, **39**, 429-444, doi: 10.1016/j.atmosenv.2004.09.065. [Link]

Jiménez, P., O. Jorba, R. Parra, and J. M. Baldasano, 2006: Evaluation of MM5-EMICAT2000-CMAQ performance and sensitivity in complex terrain: High-resolution application to the northeastern Iberian Peninsula. *Atmos. Environ.*, **40**, 5056-5072, doi: 10.1016/j.atmosenv.2005.12.060. [Link]

Khiem, M., R. Ooka, H. Hayami, H. Yoshikado, H. Huang, and Y. Kawamoto, 2010: Process analysis of ozone formation under different weather conditions over the Kanto region of Japan using the MM5/CMAQ modelling system. *Atmos. Environ.*, **44**, 4463-4473, doi: 10.1016/j.atmosenv.2010.07.038. [Link]

Lin, C. Y., Z. Wang, C. C. K. Chou, C. C. Chang, and S. C. Liu, 2007: A numerical study of an autumn high ozone episode over southwestern Taiwan. *Atmos. Environ.*, **41**, 3684-3701, doi: 10.1016/j.atmosenv.2006.12.050. [Link]

Liu, H. P. and J. C. L. Chan, 2002: Boundary layer dynamics associated with a severe air-pollution episode in Hong Kong. *Atmos. Environ.*, **36**, 2013-2025, doi: 10.1016/S1352-2310(02)00138-3. [Link]

Lu, R. and R. P. Turco, 1995: Air pollutant transport in a coastal environment - II. Three-dimensional simulations over Los Angeles Basin. *Atmos. Environ.*, **29**, 1499-1518, doi: 10.1016/1352-2310(95)00015-Q. [Link]

Russell, A. and R. Dennis, 2000: NARSTO critical review of photochemical models and modeling. *Atmos. Environ.*, **34**, 2283-2324, doi: 10.1016/S1352-2310(99)00468-9. [Link]

Shi, C., H. J. S. Fernando, and J. Yang, 2009: Contributors to ozone episodes in three U.S./Mexico border twin-cities. *Sci. Total Environ.*, **407**, 5128-5138, doi: 10.1016/j.scitotenv.2009.05.046. [Link]

Song, S. K., Z. H. Shon, Y. K. Kim, C. H. Kim, S. Y. Yoo, and S. H. Park, 2009: Characteristics of malodor pollutants and aromatic VOCs around an urban valley in Korea. *Environ. Monit. Assess.*, **157**, 259-275, doi: 10.1007/s10661-008-0533-x. [Link]

Song, S. K., Y. K. Kim, and Z. H. Shon, 2010a: Meteorological and chemical behavior of gaseous sulfur compounds in and around an Urban Valley. *Terr. Atmos. Ocean. Sci.*, **21**, 971-983, doi: 10.3319/TAO.2010.04.28.01(A). [Link]

Song, S. K., Z. H. Shon, Y. K. Kim, Y. H. Kang, I. B. Oh, and C. H. Jung, 2010b: Influence of ship emissions on ozone concentrations around coastal areas during summer season. *Atmos. Environ.*, **44**, 713-723, doi: 10.1016/j.atmosenv.2009.11.010. [Link]

Starcrest Consulting Group, LLC, 2009: 2007 Goods Movement Air Emissions Inventory at the Port of Houston, Final Draft, 34-46, Port of Houston Authority.

Tsai, D. M. and Y. L. Wu, 2006: Effects of highway networks on ambient ozone concentrations - A case study in southern Taiwan. *Atmos. Environ.*, **40**, 4004-4015, doi: 10.1016/j.atmosenv.2006.01.059. [Link]

US EPA (United States Environmental Protection Agency), 1991: Guideline for regulatory application of the Urban Airshed Model. EPA Report No. EPA-450/4-91-013.

Wang, X., Y. Zhang, Y. Hu, W. Zhou, K. Lu, L. Zhong, L. Zeng, M. Shao, M. Hu, and A. G. Russell, 2010: Process analysis and sensitivity study of regional ozone formation over the Pearl River Delta, China, during the PRIDE-PRD2004 campaign using the Community Multiscale Air Quality modeling system. *Atmos. Chem. Phys.*, **10**, 4423-4437, doi: 10.5194/acp-10-4423-2010. [Link]

Yu, S., R. Mathur, D. Kang, K. Schere, and D. Tong, 2009: A study of the ozone formation by ensemble back trajectory-process analysis using the Eta-CMAQ forecast model over the northeastern U.S. during the 2004 ICARTT period. *Atmos. Environ.*, **43**, 355-363, doi: 10.1016/j.atmosenv.2008.09.079. [Link]